Increased Global Land Carbon Sink Due to Aerosol-Induced Cooling

Yuan Zhang, Daniel S Goll, Ana Bastos, Yves Balkanski, Olivier Boucher, Alessandro Cescatti, Mark Collier, Thomas Gasser, Josefine Ghattas, Laurent Li, et al.

Global Biogeochemical Cycles

RESEARCH ARTICLE
10.1029/2018GB006051

Increased Global Land Carbon Sink Due to Aerosol-Induced Cooling

Yuan Zhang[1,2], Daniel Goll[1], Ana Bastos[1], Yves Balkanski[1], Olivier Boucher[2], Alessandro Cescatti[3], Mark Collier[4], Thomas Gasser[5], Josefine Ghattas[2], Laurent Li[2], Shilong Piao[6], Nicolas Viovy[1], Dan Zhu[1], and Philippe Ciais[1]

[1]Laboratoire des Sciences du Climat et de l'Environnement (LSCE), IPSL, CEA/CNRS/UVSQ, Gif sur Yvette, France, [2]Laboratoire de Météorologie Dynamique, IPSL, Sorbonne Université/CNRS, Paris, France, [3]Institute for Environment and Sustainability, Joint Research Centre, European Commission, Ispra, Italy, [4]CSIRO Oceans and Atmosphere, Aspendale, Victoria, Australia, [5]International Institute for Applied Systems Analysis, Laxenburg, Austria, [6]Sino-French Institute for Earth System Science, College of Urban and Environmental Sciences, Peking University, Beijing, China

Abstract Anthropogenic aerosols have contributed to historical climate change through their interactions with radiation and clouds. In turn, climate change due to aerosols has impacted the C cycle. Here we use a set of offline simulations made with the Organising Carbon and Hydrology In Dynamic Ecosystems (ORCHIDEE) land surface model driven by bias-corrected climate fields from simulations of three Coupled Model Intercomparison Project Phase 5 (CMIP5) Earth system models (ESMs; IPSL-CM5A-LR, CSIRO-Mk3.6.0, and GISS-E2-R) to quantify the climate-related impacts of aerosols on land carbon fluxes during 1860–2005. We found that climate change from anthropogenic aerosols (CCAA) globally cooled the climate, and increased land carbon storage, or cumulative net biome production (NBP), by 11.6–41.8 PgC between 1860 and 2005. The increase in NBP from CCAA mainly occurs in the tropics and northern midlatitudes, primarily due to aerosol-induced cooling. At high latitudes, cooling caused stronger decrease in gross primary production (GPP) than in total ecosystem respiration (TER), leading to lower NBP. At midlatitudes, cooling-induced decrease in TER is stronger than that of GPP, resulting in NBP increase. At low latitudes, NBP was also enhanced due to the cooling-induced GPP increase, but precipitation decline from CCAA may negate the effect of temperature. The three ESMs show large divergence in low-latitude CCAA precipitation response to aerosols, which results in considerable uncertainties in regional estimations of CCAA effects on carbon fluxes. Our results suggest that better understanding and simulation of how anthropogenic aerosols affect precipitation in ESMs is required for a more accurate attribution of aerosol effects on the terrestrial carbon cycle.

Key Points:
- Offline simulations on the ORCHIDEE model are used to investigate land C fluxes under different aerosol scenarios using CMIP5 climate
- Anthropogenic aerosols have increased global land NBP by 11.6–41.8 PgC between 1860 and 2005, mainly through their cooling effects
- Poor understandings in low-latitude precipitation response to aerosols lead to large uncertainties on aerosol impacts on NBP

Supporting Information:
- Supporting Information S1

Correspondence to:
Y. Zhang,
yuan.zhang@lmd.jussieu.fr

Citation:
Zhang, Y., Goll, D., Bastos, A., Balkanski, Y., Boucher, O., Cescatti, A., et al. (2019). Increased global land carbon sink due to aerosol-induced cooling. *Global Biogeochemical Cycles*, *33*. https://doi.org/10.1029/2018GB006051

Received 8 AUG 2018
Accepted 30 JAN 2019
Accepted article online 7 FEB 2019

1. Introduction

Aerosols have considerable impacts on climate through their direct impact on radiation transfer, as well as through aerosol-cloud interactions (Bellouin et al., 2011; Haywood & Boucher, 2000). According to the Fifth Assessment Report of Intergovernmental Panel on Climate Change (IPCC AR5), aerosols emitted by human activities caused a −0.9 (−1.9 to −0.1) W/m^2 radiative forcing, partly offsetting the global warming due to anthropogenic greenhouse gases (Boucher et al., 2013). Because terrestrial ecosystems are sensitive to climate, the climate change from anthropogenic aerosols (hereafter CCAA) will affect land surface carbon (C) fluxes, which will in turn alter the climate through the climate-carbon cycle feedbacks (Jones et al., 2003; Mahowald, 2011). The effect of CCAA on terrestrial and oceanic carbon storage is implicitly included in Earth system model (ESM) fully coupled simulations but rarely isolated from other effects, nor are its mechanisms well understood. This low level of understanding hinders our ability to assess the full impact of aerosol emissions on the climate system and therefore the indirect implications of reduced aerosol emissions, in particular in relation to air quality improvement policies that will likely reduce aerosols in the near future.

Anthropogenic aerosols (AA) perturb the terrestrial C balance through several mechanisms. First, terrestrial ecosystems respond to CCAA caused by aerosol-radiation and aerosol-cloud interactions (Jones et al., 2003; Mahowald, 2011). Second, aerosols change the quality of radiation with increased scattering and a higher fraction of diffuse light, which can penetrate deeper into vegetation canopies than can direct light. Upper

levels of canopy are often light saturated; thus, ecosystems with deep canopies respond with higher gross primary production (GPP) to more diffuse light (Gu et al., 2003; Mercado et al., 2009). Third, some aerosols contain nutrients such as nitrogen (N) or phosphorus in forms that can be utilized by plants. Deposition of these nutrients has been suggested to have fertilized current ecosystems and change the C balance (Magnani et al., 2007; Mahowald et al., 2017; Wang et al., 2017) and to partly alleviate N limitations (Luo et al., 2004; Norby et al., 2010). Additionally, aerosols decrease soil pH through N and sulfur (S) deposition, which may accelerate leaching and reduce the availability of nutrients to plants, leading to C loss (Bowman et al., 2008). Furthermore, sulfate aerosols can oxidize photosynthesis tissues (Eliseev, 2015), and other aerosols affect the photochemical processes producing near-surface ozone (Xing et al., 2017), which impairs stomatal conductance and photosynthesis (Sitch et al., 2007).

Due to the complexity of terrestrial ecosystems and the interactions between processes related to AA, separating the impacts of AA from other factors on historical changes in the land C balance using observations and statistical methods is almost impossible. Process-based models provide a way to estimate the effects of AA on the terrestrial C cycle through factorial simulation experiments. Currently, most land surface models (LSMs) do not simulate nutrient cycling or diffuse light effects on the canopy; thus, they cannot be used to investigate the full impacts of aerosols on the terrestrial C cycle. Previous studies reached contradictory conclusions about the response of the terrestrial C sink to aerosols. Using the HadCM3L ESM, Jones et al. (2003) showed that CCAA have triggered a large C sink, which was explained by suppressed soil respiration under cooler climate. Using the Community Climate System Model, CCSM3.1, Mahowald et al. (2011) found a very small global C flux response to CCAA. This discrepancy may relate to uncertainties both in how climate models simulate CCAA and in how the LSMs represent the carbon cycle processes responding to CCAA.

A well-known set of climate model simulation experiments is from the Coupled Model Intercomparison Project Phase 5 (CMIP5; Taylor et al., 2012). One of the core experiments of CMIP5 is the historical experiment (*hist*), which simulates the evolution of the Earth system driven over the historical period (1850–2005) by all natural and anthropogenic forcings. Two of the CMIP5 ESMs, IPSL-CM5A-LR and CSIRO-MK3.6.0 (hereafter referred to as IPSL and CSIRO) further provided experiments similar to *hist* with the exception that the radiative effects of AA were omitted (hereafter referred to as *NoAA*). The comparison of the *hist* and *NoAA* experiments allows investigating the climate effects of AA on terrestrial C fluxes. The GISS-E2-R ESM (hereafter referred to as GISS) provided an experiment without the radiative effect of all aerosols (hereafter referred to as *NoA*). Considering that the effects of AA and all aerosols on climate are similar (see section 3.1), in order to include more ESMs and assess the uncertainties, the GISS model is also considered. For the sake of simplicity, we hereafter refer to CCAA and AA for all three ESMs, even though it does not strictly apply to GISS.

Using the climate simulations from the *hist* and *NoAA*/*NoA* scenarios from the three CMIP5 ESMs, we aim to estimate the terrestrial C flux change caused by CCAA during the period 1860–2005 using a single process-based LSM, Organising Carbon and Hydrology In Dynamic Ecosystems (ORCHIDEE). The main objectives of this study are (1) to quantify the impacts of CCAA on land C fluxes, as modeled by ORCHIDEE, at global and regional scales; (2) to evaluate how uncertainty in CCAA simulated by ESMs translates into uncertainty in C fluxes in ORCHIDEE; and (3) to understand the mechanisms behind these impacts and uncertainties.

2. Data and Methods

2.1. ORCHIDEE Model

The ORCHIDEE model is the LSM component of the Institute Pierre-Simon Laplace (IPSL) ESM. ORCHIDEE represents key energy, water, and biogeochemical processes in terrestrial ecosystems (Krinner et al., 2005) and is mainly based on three components: the Surface-vegetation-atmosphere transfer SECHIBA (Schématisation des Echanges Hydriques à l'Interface entre la Biosphère et l'Atmosphère) model, dealing with energy and hydrological processes (De Rosnay & Polcher, 1998; Ducoudré et al., 1993); the Lund-Potsdam-Jena dynamic global vegetation model, LPJ, which simulates the dynamics of natural vegetation (Sitch et al., 2003); and the STOMATE (Saclay Toulouse Orsay Model for the Analysis of Terrestrial Ecosystems) model, which models the main biogeochemical and related processes (e.g., photosynthesis, carbon allocation, respiration, and phenology; Krinner et al., 2005). Detailed descriptions of the parameterizations of the main processes in ORCHIDEE can be found in Krinner et al. (2005) and Piao et al. (2009).

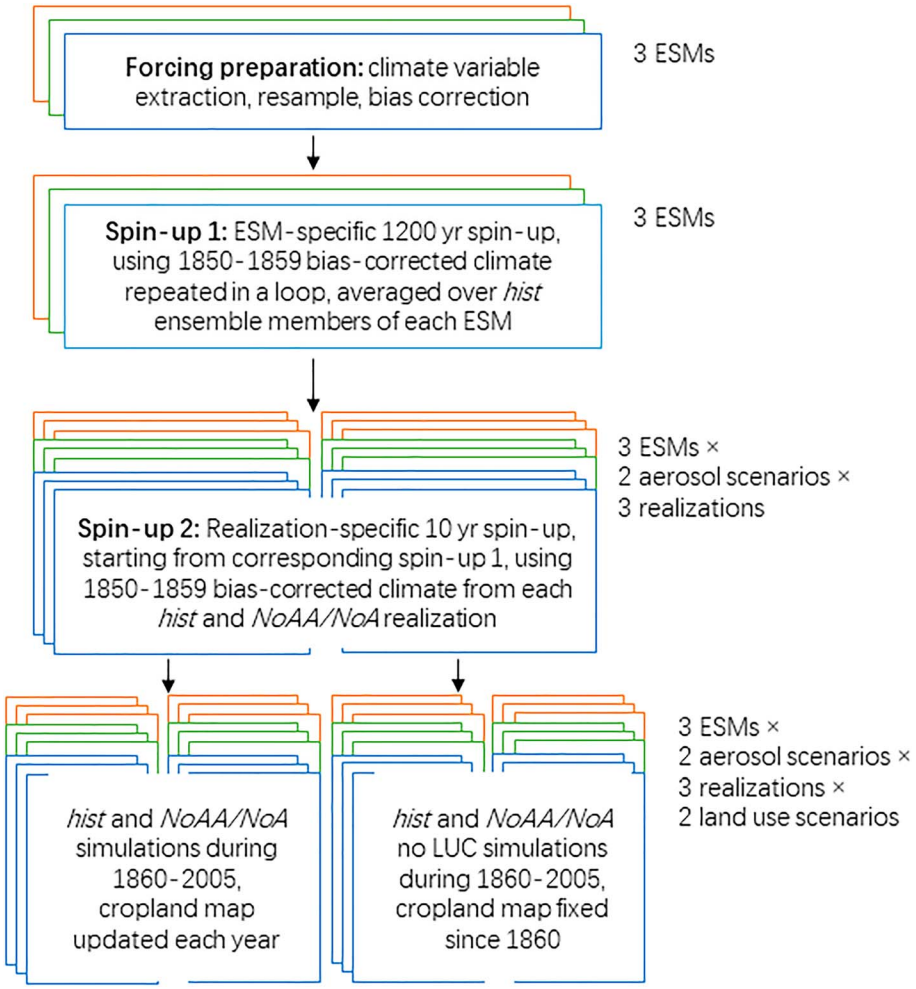

Figure 1. Schematic of the spin-up and simulations. ESM = Earth system model.

ORCHIDEE has been tested at various spatial-temporal scales using in situ measurements from different plant functional types and satellite observations (Ciais et al., 2005; Krinner et al., 2005; Piao et al., 2006; Traore et al., 2014) and has been widely applied to estimate global and regional C budgets (Le Quéré et al., 2017; Piao et al., 2009) and to investigate the biogeochemical consequences of climate trends and extremes (Ciais et al., 2005; Piao, Ciais, et al., 2009; Reichstein et al., 2007).

Here we use ORCHIDEE version v4220 in offline mode (i.e., the model output does not affect climate forcing), with the setup configurations described in the next section and in Figure 1. It should be noted that the differential direct and diffuse light transmission scheme remains unavailable for the current ORCHIDEE version, nor does the model simulate effects of nutrient deposition.

2.2. Forcing Data and Experiments Setup

2.2.1. ESM Simulations

Climate data used to drive ORCHIDEE are derived from simulations of three CMIP5 ESMs that documented separately climate change with and without AA/aerosols (*hist* and *NoAA*/*NoA*), including the IPSL ESM (IPSL-CM5A-LR; Dufresne et al., 2013), the CSIRO ESM (CSIRO-Mk3.6.0; Jeffrey et al., 2013; Rotstayn et al., 2012), and the GISS ESM (GISS-E2-R; Miller et al., 2014; Schmidt et al., 2014). Furthermore, three realizations (i.e., perturbed initial conditions) of the *hist* and *NoAA*/*NoA* experiments of each ESM are used (Table S1). Under the CMIP5 protocol, the *hist* experiment uses simulations driven by all observation-based natural and anthropogenic forcings, including AA emissions. While for *NoAA*/*NoA* simulations, the forcings

remain the same as those for *hist* simulations except that aerosol emissions are prescribed at the preindustrial level (AA for *NoAA*, whereas all aerosol emissions for *NoA* in GISS). All ESMs simulate the radiative effects of aerosol species including dust, sea salt, sulfate, black carbon, and organic carbon. The GISS model additionally considered nitrate aerosols. All ESMs include the direct radiative effect (i.e., light absorption and scattering) on climate and the indirect effect of aerosols on climate by changing cloud albedo. The CSIRO model also includes aerosols' impact of a reduction of cloud droplet size on the precipitation efficiency.

The climate variables required to drive ORCHIDEE are daily or higher-frequency air temperature maximum (*Tmax*) and minimum (*Tmin*), precipitation (*Precip*), downward surface shortwave radiation (*SWdown*), downward surface longwave radiation (*LWdown*), near-surface specific humidity (*Qair*), air pressure (*Ps*), and near-surface (10 m) zonal (*Wind_E*) and meridional (*Wind_N*) wind components. These climate variables are further interpolated to 30-min time steps in ORCHIDEE for flux simulations. We obtained the climate variables at daily resolution from IPSL and CSIRO output under *hist* and *NoAA* scenarios from the Earth System Grid Federation node (https://esgf-node.ipsl.upmc.fr/projects/esgf-ipsl/) or directly from the modeling centers. For GISS, daily output since 1850 is available from only one *hist* realization (CMIP5 GISS-E2-R r6i1p3), while the other *hist* and *NoA* realizations only provide monthly data. Here we calculated the daily climate anomalies in each month using GISS r6i1p3 data and added them to the monthly data of the other *hist* and *NoA* realizations. All data are regridded to 2° × 2°. Apart from climate, global annual atmospheric CO_2 concentration is also required as an input ORCHIDEE, and is taken from an ice core and National Oceanic and Atmospheric Administration monitoring station data (https://www.esrl.noaa.gov/gmd/ccgg/trends/).

2.2.2. Bias Correction

The response of terrestrial ecosystems to climate change depends on background climate (Ahlström et al., 2017; Sitch et al., 2008; Wang et al., 2014). Since ESMs have bias in their simulated climate compared with observations (Flato et al., 2013), systematic errors in simulated C fluxes with ORCHIDEE could be introduced if the ESM output is not corrected for its biases. The impact of such bias in ESM climate on C fluxes and pools was nicely illustrated in Ahlström et al. (2017) for precipitation over the Amazon, for instance. Therefore, we corrected biases in ESM preindustrial climate at a pixel level using the observation-based reanalysis data set CRU-NCEP (Climatic Research Unit-National Centers for Environmental Prediction; version 7.2) at 2° × 2° resolution and 6-hourly time steps for the period 1901–2016 (available online at: https://vesg.ipsl.upmc.fr/thredds/catalog/store/p529viov/cruncep/V72_1901_2016/catalog.html). For each ESM simulation, *Tmax*, *Tmin*, *Wind_N*, *Wind_E*, and *Ps* are corrected as follows:

$$V_{\mathrm{corr}}(t,m) = V_{\mathrm{mod}}(t,m) - \Delta V(m) \tag{1}$$

$$\Delta V(m) = V_{\mathrm{base},hist}(m) - V_{\mathrm{base,obs}}(m) \tag{2}$$

while *Precip*, *SWdown*, *LWdown*, and *Qair* are corrected as follows:

$$V_{\mathrm{corr}}(t,m) = V_{\mathrm{mod}}(t,m) / \Delta V(m) \tag{3}$$

$$\Delta V(m) = V_{\mathrm{base},hist}(m) / V_{\mathrm{base,obs}}(m) \tag{4}$$

where $V_{\mathrm{corr}}(t,m)$ is the corrected climate variable at day t of month m, $V_{\mathrm{mod}}(t,m)$ is the CMIP5 climate output at time t of month m, and $V_{\mathrm{base,\ obs}}(m)$ is the climate baseline from observations (here CRU-NCEP data) in month m, calculated as the average climate in month m during the first 10 years of this data set (1901–1910). $V_{\mathrm{base,\ }hist}(m)$ is the modeled climate baseline of month m, which is ESM dependent and calculated during 1850–1859 using the average climate across the three ensemble members of *hist* simulations. Here we correct the ESM baseline from 1850 to 1859 using CRU-NCEP data from 1901 to 1910. This mismatch in the baseline period is unavoidable because the CRU-NCEP data set begins in 1901. Nevertheless, it should not cause large errors because the simulated climate change between the two periods is small (<0.19 °C in surface temperature or *Tair*, <10 mm in *Precip*, and <1.2 W/m^2 in *SWdown*) compared with that during the entire study period of 1850–2005 (Figure 2). This is due to relatively low anthropogenic forcing level prior to 1900.

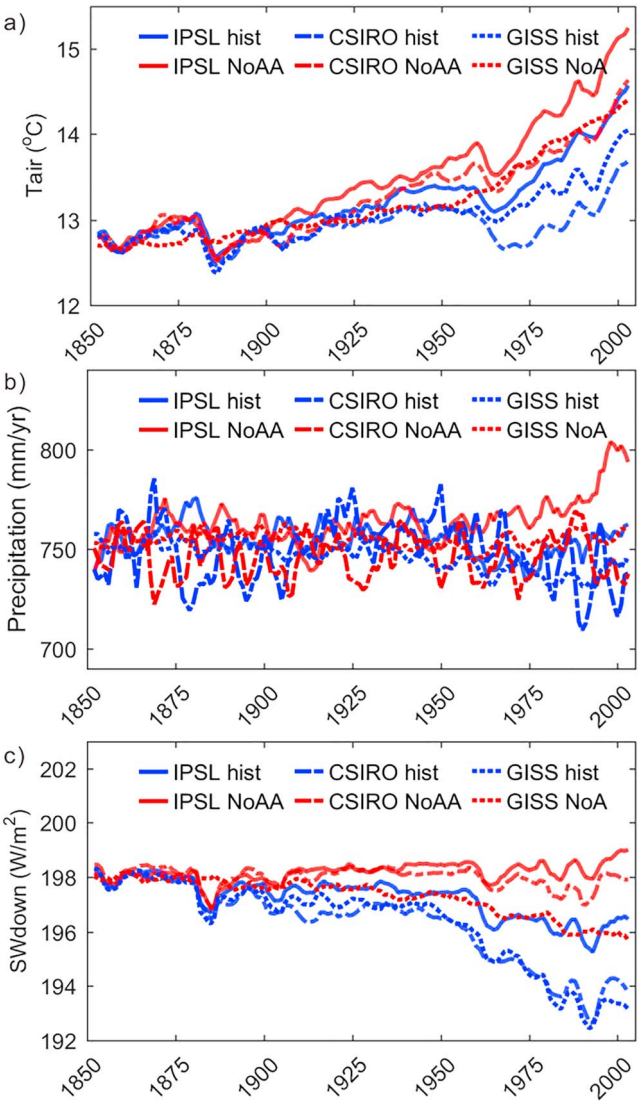

Figure 2. Global average bias-corrected terrestrial (a) air temperature, (b) precipitation and (c) incoming shortwave radiation (*SWdown*) under the *hist* (blue) and *NoAA/NoA* (red) scenarios for IPSL (solid lines), CSIRO (dashed lines), and GISS (dotted lines). Five-year moving average was applied to all variables.

2.2.3. Experimental Design

Because of the high computational demand of the LSM to equilibrate land carbon cycle to the initial climate state (1850–1859), and the rather small differences in the initial climate between the bias-corrected ensemble members and between the *hist* and *NoAA/NoA* scenarios (Figure 2), we used a two-step spin-up scheme to equilibrate the carbon cycle (Figure 1). First, for each ESM, a long spin-up of 1,200 years was performed with ORCHIDEE driven by a 10-year climate sequence (1850–1859) repeated in a loop to bring all C pools to equilibrium. To construct this 10-year climate, we averaged the bias-corrected ESM climate over *hist* ensemble members from each ESM. We have checked that the 10-year period has no anomalous decadal variability (Figure 2). Then, a 10-year short spin-up starting from the end of the first spin-up using 1850–1859 climate from each *hist* or *NoAA/NoA* ensemble member was used to adjust the C pools with fast turnover (e.g., leaf and litter C pools) to the corresponding climate. Since AA emissions remain small during this period, the initial C pools from the *NoAA/NoA* simulations are not significantly different from the *hist* simulations (Figure S1).

After the two-step spin-up, two simulations with ORCHIDEE for the period 1860–2005 were performed with the bias-corrected climatic forcing and different land use scenarios (Figure 1). One simulation used a cropland distribution updated each year according to LUH2v2h (Land Use Harmonization)-based LC_CCI (The ESA Land Cover Climate Change Initiative) plant functional type (Hurtt et al., 2011; Poulter et al., 2015), while the other simulation fixed the cropland distribution to the one of 1860 (natural vegetation being simulated by the dynamic global vegetation model module). By comparing results from the two simulations, we can quantify the C flux caused by land use change (land use emissions) and by climate and CO_2 changes (natural sink). Altogether, 3 ESMs × 2 aerosol scenarios × 3 ESM ensemble members × 2 land use scenarios were considered, making a total of 36 different ORCHIDEE runs. A detailed experiment setup is shown in Table 1.

2.3. Analyses

The analysis is based on C fluxes averaged among the three realizations to represent each experiment in Table 1. To investigate how the C fluxes are affected by different climate variables and atmospheric CO_2, a multiple regression approach was used to decompose the C flux time series to the effects of different climate factors, following the method of Piao et al. (2013):

$$Y = a\times Tair + b\times Precip + c\times SWdown + d\times CO_2 + e + \varepsilon \quad (5)$$

where Y is the C fluxes and a, b, c, and d are the sensitivities of target C flux to temperature, precipitation, shortwave radiation, and CO_2 concentration, respectively.

Then, the contribution of climate variable V to C flux (Y) can be written as

$$\Delta Y_V = S\times \Delta V \quad (6)$$

where ΔY_V is the contribution of a given climatic factor V to the difference in C flux between the end (1996–2005) and beginning (1860–1869) of the study period. S is the sensitivity of the corresponding factor calculated in equation (5), and ΔV is the change of the climate factor during the same period. The C flux

Table 1
The Climate and Land Use Scenarios for Each Experiment

Experiment name	Number of realizations	Climate scenario	Cropland map
IPSL *hist*	3	IPSL historical[a]	Time varying
IPSL *hist NoLUC*	3	IPSL historical	Fixed at 1860
IPSL *NoAA*	3	IPSL historicalNoAA[b]	Time varying
IPSL *NoAA NoLUC*	3	IPSL historicalNoAA	Fixed at 1860
CSIRO *hist*	3	CSIRO historical	Time varying
CSIRO *hist NoLUC*	3	CSIRO historical	Fixed at 1860
CSIRO *NoAA*	3	CSIRO historicalNoAA	Time varying
CSIRO *NoAA NoLUC*	3	CSIRO historicalNoAA	Fixed at 1860
GISS *hist*	3	GISS historical	Time varying
GISS hist *NoLUC*	3	GISS historical	Fixed at 1860
GISS *NoA*	3	GISS historicalNoA[c]	Time varying
GISS *NoA NoLUC*	3	GISS historicalNoA	Fixed at 1860

[a](Climate from simulations driven by all natural and anthropogenic forcings). [b](Same as historical, but anthropogenic aerosol emissions are prescribed at the preindustrial level). [c]Same as historical, but all aerosol emissions are prescribed at the preindustrial level.

change caused by AA through changes in climate factor V at the end of the study period, $\Delta Y_{V,\,\mathrm{aero}}$ can be diagnosed as

$$\Delta Y_{V,\mathrm{aero}} = \Delta Y_{V,hist} - \Delta Y_{V,NoAA/NoA} \tag{7}$$

This decomposition scheme is not perfect because it assumes a linear response of C fluxes to climate variables, while terrestrial ecosystems do not always behave linearly. In addition, there might be interactions between different climate factors. Nevertheless, at the interannual time scale, this simple approach has been shown to be useful to estimate the effects of different climate factors (Jung et al., 2017; Piao et al., 2013).

3. Results

3.1. Impacts of Aerosols on Climate

The evolution of the bias-corrected global climate (for convenience, all climates hereafter indicate the climate after bias correction) under the *hist* and *NoAA*/*NoA* scenarios is shown in Figure 2. Due to the bias correction, the climate states of *hist* and *NoAA/NoA* from different ESMs are similar in the 1850s.

Simulated *Tair* presents increasing trends under all the scenarios during the study period, especially after the 1960s (Figure 2a). This temperature increase is more pronounced for the *NoAA/NoA* scenarios than for the *hist* scenarios for each ESM, indicating a cooling effect of aerosols. In spite of the consistency in the sign of the AA-induced temperature change, the three ESMs show different magnitudes of the CCAA cooling effect, with the strongest land surface cooling found in CSIRO (0.75 °C in 2005), followed by IPSL (0.64 °C in 2005) and GISS (0.37 °C in 2005). Because GISS *NoA* excluded the effects of both natural aerosols (including volcanic aerosols) and AA, the difference in interannual climate variations between GISS *hist* and GISS *NoA* is larger than that between *hist* and *NoAA* from other ESMs.

In contrast to temperature, precipitation generally shows no trend in most of the simulations (Figure 2b), except that the IPSL *NoAA* ensemble average exhibits an increasing global precipitation trend after the 1960s. This trend leads to a 40-mm/year precipitation difference between IPSL *hist* and IPSL *NoAA* in the 2000s. In CSIRO and GISS, the global mean precipitation under the *hist* and *NoAA/NoA* scenarios are similar.

In terms of *SWdown*, all the three ESMs show remarkable decreasing trends after the 1960s under the *hist* scenario, while *SWdown* under the *NoAA/NoA* scenarios either remains relatively constant (IPSL *NoAA* and CSIRO *NoAA*) or decreases only slightly (GISS *NoA*; Figure 2c). These differences indicate a diming effect of aerosols. Similar to the cooling effect, the diming is stronger in CSIRO (4.8 W/m^2 in 2005) than in IPSL and GISS (both 2.7 W/m^2 in 2005).

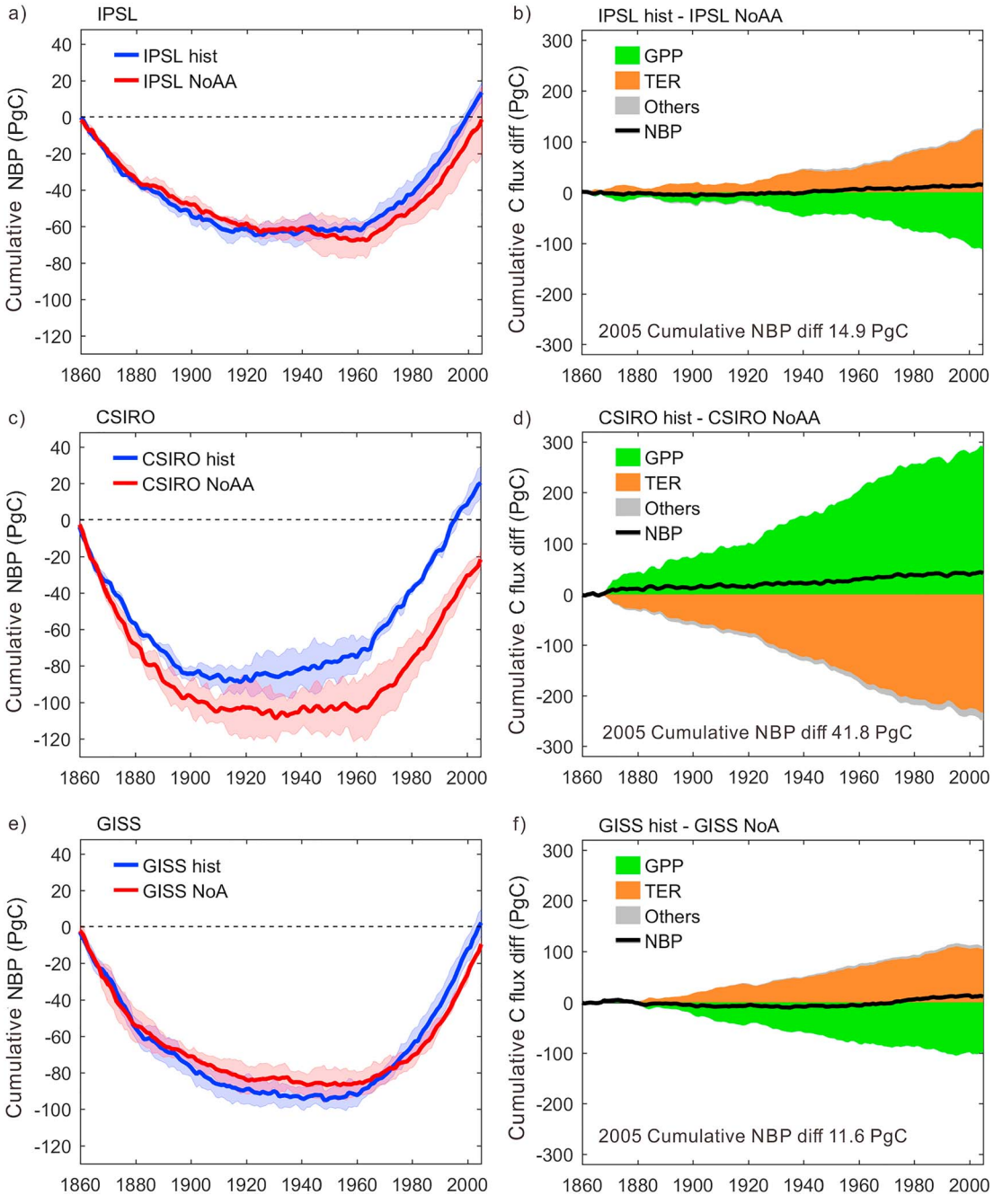

Figure 3. Cumulative terrestrial C fluxes under the *hist* and *NoAA/NoA* scenarios and their difference. (a) The cumulative terrestrial net biome production (NBP) since 1860 from the IPSL simulations. The shaded area indicates standard deviation among ensemble members. (b) The cumulative difference in gross primary production (GPP), total ecosystem respiration (TER), other C fluxes (i.e., fire and harvest), and NBP between IPSL *hist* and IPSL *NoAA*. (c, e) The same as (a) but for the CSIRO and GISS simulations, respectively. (d, f) The same as (b) but for the CSIRO and GISS simulations, respectively. Positive flux indicates flux from atmosphere to terrestrial ecosystems.

3.2. Responses of C Fluxes at the Global Scale

The global cumulative land net biome production (NBP; defined as the net flux of CO_2 from atmosphere to land) since 1860 under the *hist* and *NoAA/NoA* scenarios is shown in Figures 3a, 3c, and 3e. All the *hist* simulations show persistent land C losses before 1900 and C gains after the 1960s. At the end of the study period, a positive cumulated NBP is found (13.4 PgC for IPSL *hist*, 20.3 PgC for CSIRO *hist*, and 2.1 PgC for GISS *hist*). The magnitude of this C uptake is within the range of that assessed in IPCC AR5 (Ciais et al., 2013).

The cumulative NBP in the *NoAA/NoA* simulations showed a U-shape curve similar to that in the *hist* simulations (Figures 3a, 3c, and 3e). However, at the end of the study period, the cumulative *NoAA/NoA* NBP is negative, that is, a net loss of CO_2 from the land to the atmosphere (−1.5 PgC for IPSL *NoAA*, −21.5 PgC for CSIRO *NoAA*, and −9.4 PgC for GISS *NoA*). The difference between *hist* and *NoAA/NoA* on cumulative NBP is mainly due to a weaker C sink in *NoAA/NoA* after the 1960s. For CSIRO, there is also a more pronounced C loss in the *NoAA* than *hist* scenario before 1960.

Differences in gross C fluxes of GPP and total ecosystem respiration (TER) during 1860–2005 between the *hist* and *NoAA* simulations, that is, CCAA-induced changes in these fluxes, are illustrated in Figures 3b, 3d, and 3f. For the IPSL and GISS models, CCAA cause a small decrease in both GPP and TER (Figures 3b and 3f). The GPP decrease (0.77 PgC/year for IPSL and 0.68 PgC/year for GISS) is smaller than the decrease in TER and other emissions (e.g., fires, harvest, or direct C loss from land use change; 0.87 PgC/year for IPSL and 0.76 PgC/year for GISS), leading to an NBP increase, that is, a larger sink due to CCAA (0.10 PgC/year for IPSL and 0.08 PgC/year for GISS). In contrast, the CCAA of the CSIRO model cause a positive response of GPP and TER and other emissions (Figure 3d). However, due to a larger increase in GPP (on average 1.99 PgC/year) than in TER and other emissions (on average 1.71 PgC/year), NBP increases due to CCAA in the CSIRO model as well (0.29 PgC/year). Bear in mind that these results depend on the response of ORCHIDEE to CCAA and could be qualitatively and quantitatively different with another LSM.

3.3. Responses of C Fluxes at Different Latitudes

To identify the regions that compose the above global difference in CCAA-induced GPP and TER changes among the three ESMs, we analyze changes in different latitude bands during 1966–2005 in Figure 4. This period was selected because it shows the strongest CCAA (Figure 2).

At southern midlatitudes (30–60°S; Figure 4), IPSL and CSIRO show positive impacts of CCAA on GPP and TER. Due to the larger increase in GPP than in TER, CCAA triggered an increase of NBP of 46 TgC/year for IPSL and 23 TgC/year for CSIRO during 1966–2005. However, for GISS, both GPP and TER decreased slightly, and a 1 TgC/year NBP increase is found in response to CCAA during 1966–2005. An investigation of CCAA during the same period shows that aerosols caused an increase in precipitation in IPSL and CSIRO but a small decrease in precipitation in GISS (Figure S11).

The largest differences among ESMs are found at low latitudes (30°S–30°N; Figure 4). For IPSL, CCAA caused declines in both GPP and TER (Figure 4a), while for CSIRO and GISS, CCAA increased GPP and TER (Figures 4b and 4c). For the CSIRO model, the increase of GPP and TER simulated by ORCHIDEE is 5 times larger than for GISS. Although the GPP and TER responses to CCAA diverge among ESMs, all the simulations indicate a positive NBP response to CCAA in the low latitudes during 1966–2005 (42 TgC/year for IPSL, 353 TgC/year for CSIRO, and 369 TgC/year for GISS). The magnitude of the NBP response at low latitudes is 1 order of magnitude larger than in the other latitude bands for CSIRO and GISS, while it is comparable for IPSL.

At northern middle (30–60°N) and high (60–90°N) latitudes (Figure 4), the CCAA from all the three ESMs result in declines in both GPP and TER. These GPP and TER responses to CCAA are opposite to those in southern midlatitudes for IPSL and CSIRO, which might be due to the opposite response of precipitation to aerosols in the two latitudinal bands (Figure S11). At northern midlatitudes, TER decreases more than GPP, leading to a small increase in NBP (123 TgC/year for IPSL, 2 TgC/ year for CSIRO, and 25 TgC/ year for GISS), while at northern highlatitudes, GPP decreases more than TER, causing a small NBP decrease of 31, 101, and 47 TgC/year, respectively.

Using simulations with fixed cropland maps, we decomposed the total NBP into “natural sink” and “land use emissions.” The impacts of CCAA on both fluxes are also shown in Figure 4. All ESMs in all latitudes agree that the CCAA-induced difference in the natural sink (“NoLUC” in Figure 4) is similar but slightly larger compared with the total NBP change. In contrast, the land use emissions (i.e., the difference between the total NBP and the natural sink, referred to as “LUC effect” in Figure 4) is almost insensitive to CCAA.

3.4. Spatial Pattern of NBP Difference

The spatial pattern of CCAA-caused NBP change during 1966–2005 is shown in Figures 5a, 5c, and 5e. All the ESMs generally show patterns of NBP increases at middle to low latitudes in response to CCAA,

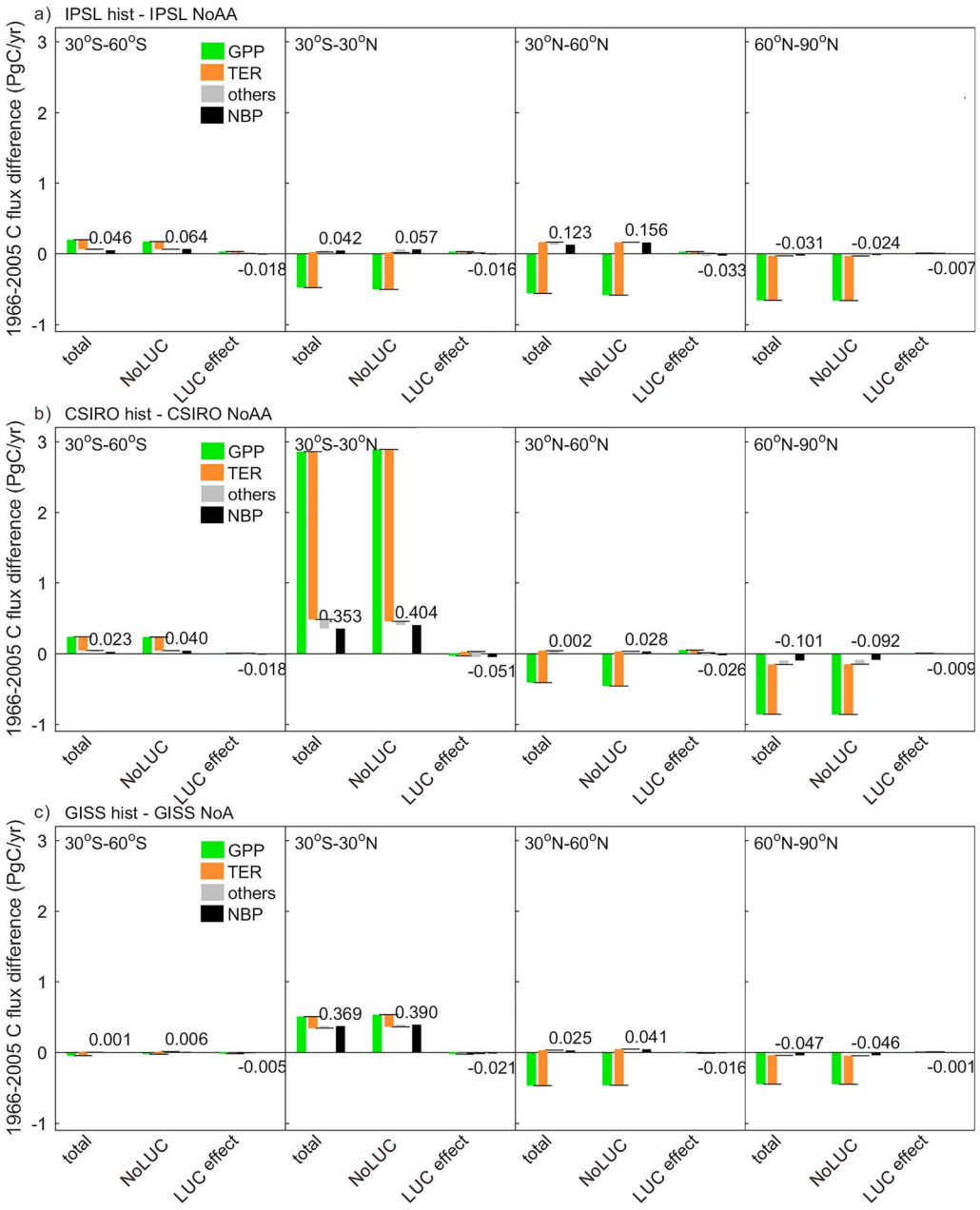

Figure 4. Difference in gross primary production (GPP), total ecosystem respiration (TER), other C fluxes (i.e., fire and harvest), and net biome production (NBP) under the *hist* and *NoAA*/*NoA* scenarios during 1966–2005 in different latitudes. (a) C flux difference from the IPSL simulations; (b) C flux difference from CSIRO simulations; and (c) C flux difference from the GISS simulations. "Total" indicates simulations with cropland map updated each year; "NoLUC" indicates simulations with fixed cropland map, indicating "natural sink" (see methods); "LUC effect" is the difference between "total" and "NoLUC," indicating the "land use emissions." The baseline of respiration and other C flux bars are indicated as short black horizontal lines. The numbers indicate the average NBP difference during 1966–2005. Positive flux indicate increase in GPP or decrease in C release (respiration and other fluxes) due to anthropogenic aerosols.

except over the eastern Amazon for IPSL and small regions in the Amazon for CSIRO. The spatial pattern of NBP change at northern high latitudes from CCAA is less consistent among ESMs. Nevertheless, all the ESMs agree that in this region more areas show negative impacts of CCAA on NBP, that is, a decreased sink or an increased source. Globally, CCAA cause NBP to increase in 55–60% of the land area and to decrease in 37–43% of the area.

To investigate which climate variables control the CCAA-induced NBP difference patterns, we show the temperature and an aridity index (precipitation-potential evapotranspiration, P-PET) changes due to

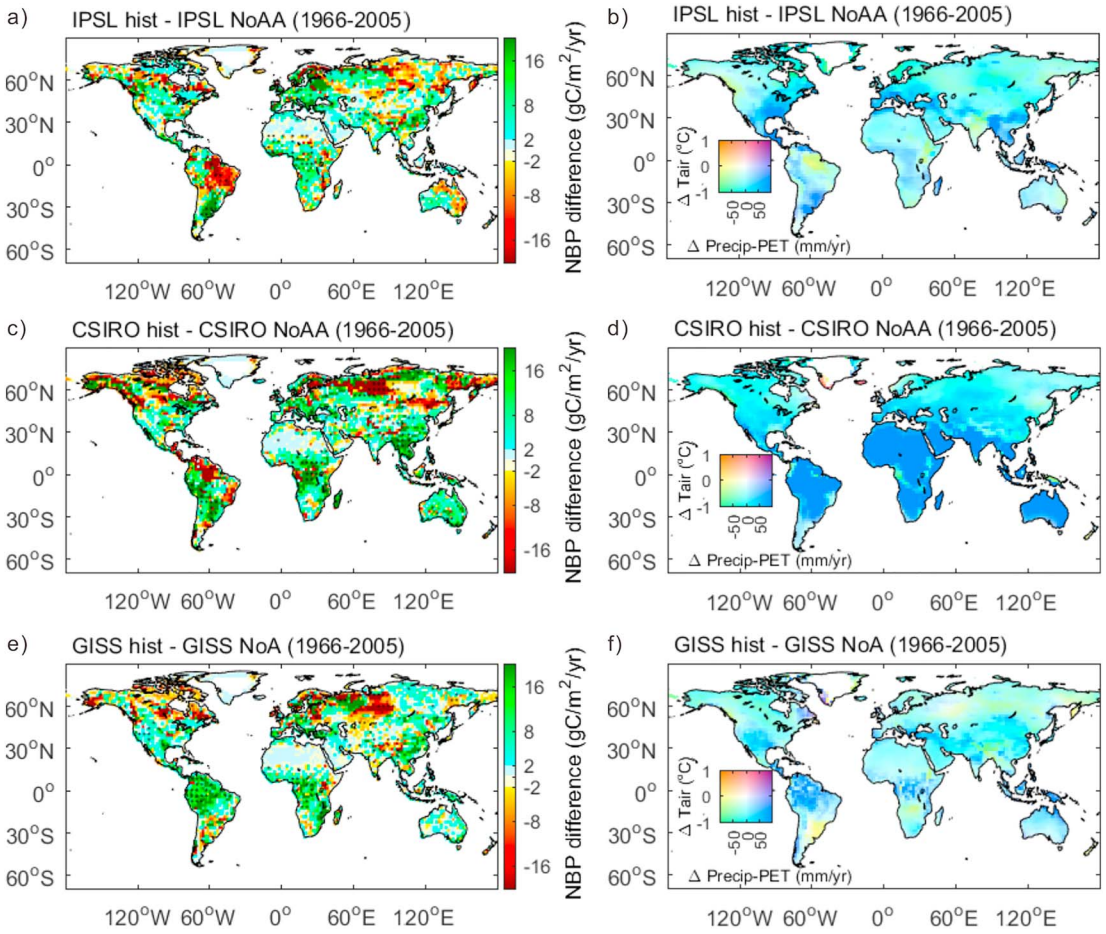

Figure 5. Spatial patterns of differences in net biome production (NBP) and climate between *hist* and *NoAA/NoA* during 1966–2005. (a) NBP difference between IPSL *hist* and IPSL *NoAA*. (b) Air temperature and precipitation-potential evapotranspiration (P-PET) differences between IPSL *hist* and IPSL *NoAA*. (c, e) The same as (a) but for CSIRO and GISS, respectively. (d, f) The same as (b) but for CSIRO and GISS, respectively. The PET is calculated following Thornthwaite (1948). Dotted areas in (a), (c), and (e) indicate significant difference between the *hist* and *NoAA/NoA* ensembles.

CCAA in Figures 5b, 5d, and 5f (*SWdown* is not shown because its contribution to CCAA is similar to temperature change). For all ESMs, a cooler temperature is the global fingerprint of CCAA. However, the response of P-PET to AA is remarkably different among ESMs. For IPSL, AA caused wetter climate in eastern North America, western South America, Argentina, central Africa, and south China, whereas it induced drier climate in eastern South America and east Australia (Figure 5b), which coincide with the mid-latitude and low-latitude NBP-increase and NBP-decrease areas from CCAA (Figure 5a). For CSIRO and GISS, P-PET decrease also matches most of the NBP-decrease regions at low latitudes (e.g., East Brazil and west equatorial Africa for CSIRO and Argentina for GISS).

In Figure 6, we investigated whether the impacts of CCAA on NBP operate mainly through changes on GPP or TER. Simulations from all the ESMs agree that in most pixels CCAA affect NBP mainly through changing GPP, regardless of whether the change is positive or negative (Figure 6). The area dominated by the GPP response accounts for 62–68% of the land area, while the area dominated by the TER response is only 28–35%. These TER-dominated areas are mainly found in east North America, as well as east Europe and central South America for IPSL.

3.5. Sensitivities of C Fluxes to Climate Factors

To understand how CCAA quantitatively affect C fluxes as simulated by ORCHIDEE, we present the sensitivities of NBP and GPP to *Tair*, *Precip*, and *SWdown* in Figures 7 and S5–S9. Similar sensitivity patterns are found between the *hist* and *NoAA/NoA* simulations and among ESMs, so that the impact of CCAA is not

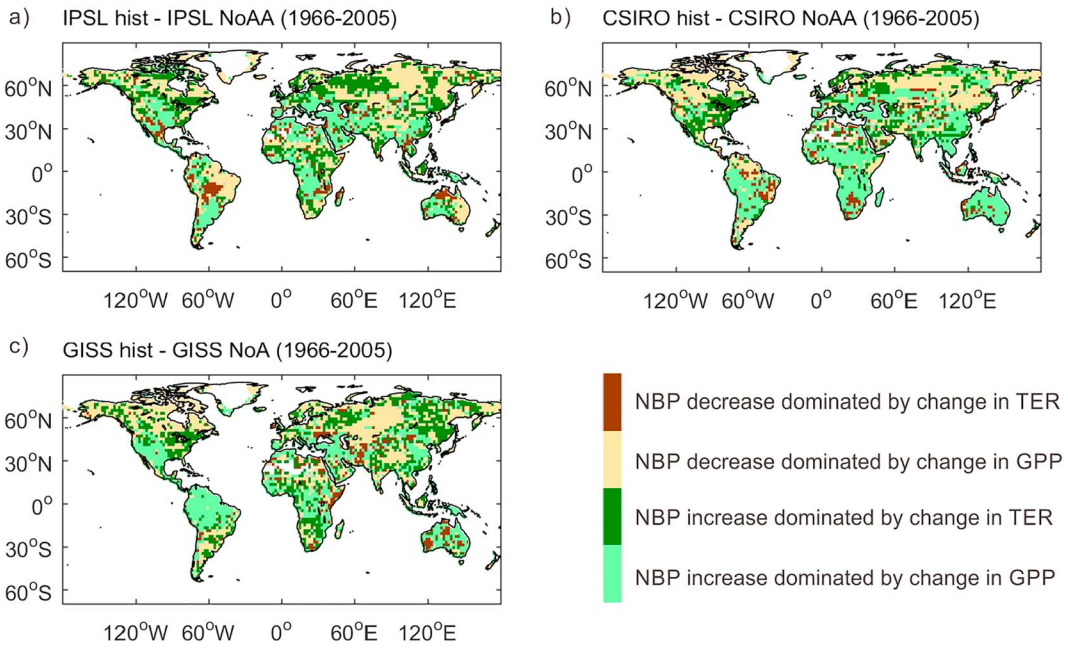

Figure 6. Spatial patterns of the main contributors (gross primary production [GPP] or total ecosystem respiration [TER]) to the net biome production (NBP) difference caused by anthropogenic aerosols during 1966–2005. (a) The main contributors for the IPSL simulations. (b, c) the same as (a) but for the CSIRO and GISS simulations, respectively. The green and red indicate NBP increase or decrease in response to aerosols. The light and dark colors indicate if the NBP difference is mainly caused by GPP or TER.

because the terrestrial C cycle sensitivity is changed but because of regional changes in *Tair*, *Precip*, and *SWdown*.

The NBP sensitivity to temperature shows a strong meridional gradient (Figure 7a). At low latitudes, NBP has strong negative sensitivity to temperature, with a magnitude of −80 $gC \cdot m^{-2} \cdot year^{-1} \cdot °C^{-1}$, while at high latitudes, NBP slightly increases with temperature (10 $gC \cdot m^{-2} \cdot year^{-1} \cdot °C^{-1}$).

Opposite to temperature, the NBP sensitivity to precipitation is generally positive in latitudes south than 60°N, whereas it becomes negative at latitudes north of 60°N (Figure 7c). The strongest positive NBP-precipitation sensitivity values are found in dry regions, such as Sahel, the central United States, middle Asia, Southern Africa, west Argentina, and Australia, with values over 6–8 $gC \cdot m^{-2} \cdot year^{-1} \cdot (10\ mm/year)^{-1}$. NBP is insensitive to precipitation in regions covered by rainforests along the equator.

In terms of NBP sensitivity to *SWdown* (Figure 7e), the ORCHIDEE simulations using the different ESM forcings generally agree that in most low-latitude regions, NBP decreases with radiation, except for rainforests in west Amazon, central Africa, and Indonesia, where light was thought to be the limiting factor of vegetation growth (Huete et al., 2006; Nemani et al., 2003; Zhang et al., 2016). In some semiarid regions (e.g., north Argentina), negative sensitivity of NBP to *SWdown* is detected, potentially because the increase in *SWdown* can increase evapotranspiration and decrease water availability. At high latitudes, the radiation sensitivity is less consistent among ESMs.

The GPP sensitivities to each climate factor show similar patterns to NBP sensitivities, but with much stronger magnitude (Figures 7b, 7d, and 7f). This similarity in sensitivity pattern is expected because GPP is found to be the dominant flux causing NBP change (Figure 6).

3.6. Dominant Climate Factors Causing NBP Change Due to AA

The decomposition shown in equations (5)–(7) allows us to investigate which climate factor contributes the most to the CCAA-induced NBP change (Figure 8). A robust meridional pattern of the main climate factors is found among ESMs.

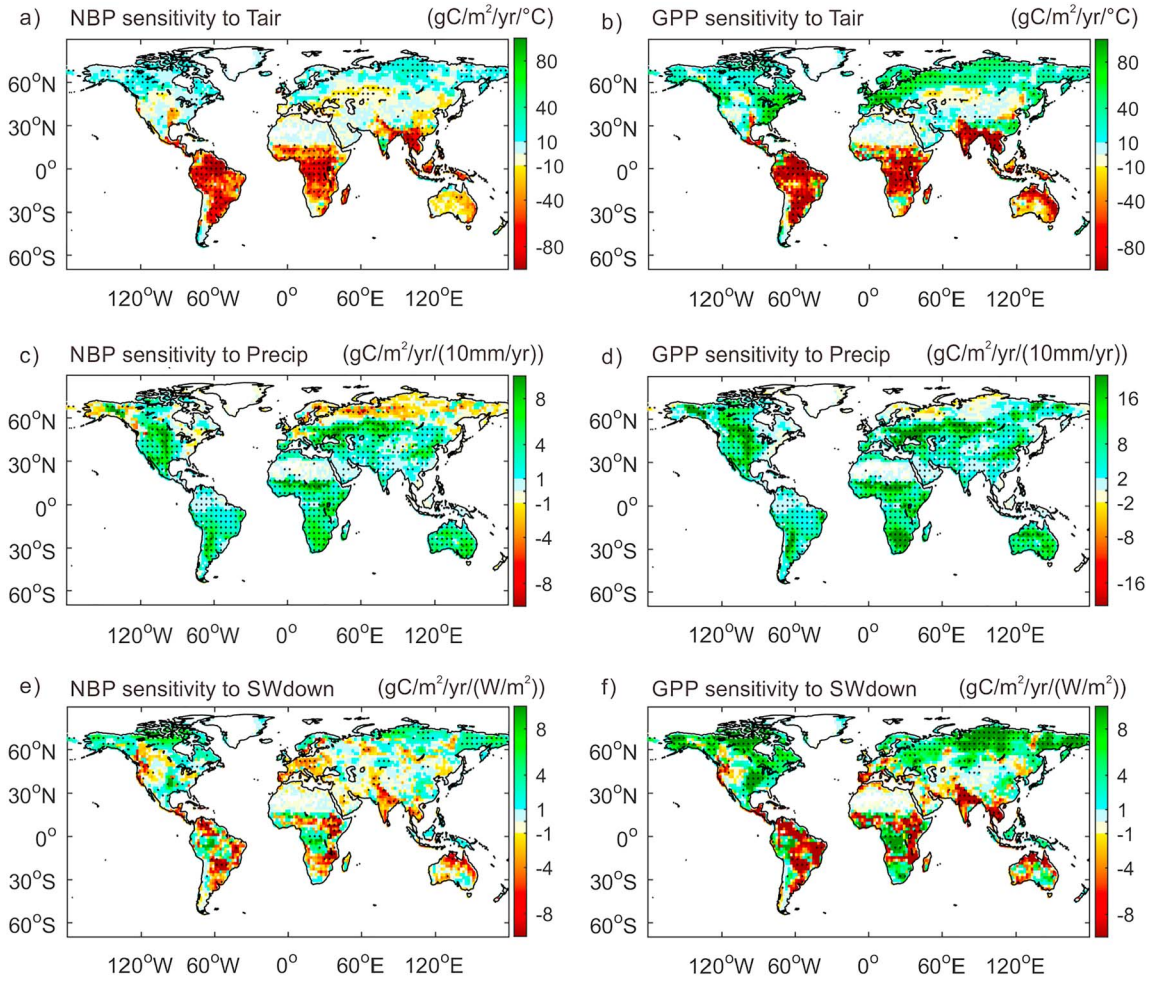

Figure 7. The sensitivity of net biome production (NBP) and gross primary production (GPP) to climate factors for IPSL *hist* simulations during 1860–2005. (a) NBP sensitivity to temperature. (b) GPP sensitivity to temperature. (c) NBP sensitivity to precipitation. (d) GPP sensitivity to precipitation. (e) NBP sensitivity to *SWdown*. (f) GPP sensitivity to *SWdown*. The dotted regions indicate where at least two of the three ensemble members detected a sensitivity significantly different from 0. The sensitivities for IPSL *NoAA* and other Earth system models are in Figures S5–S9.

At southern midlatitudes (30–60°S), the NBP change is mainly due to CCAA-related precipitation change (e.g., south Argentina and South Australia; Figures 8a, 8c, and 8e). The precipitation-dominated areas cover about 50% of this latitude band for all the three ESMs (Figures 8b, 8d, and 8f).

At low latitudes (30°S–30°N), positive and negative NBP changes cannot be attributed to a single climate factor (Figure 8). In 56–75% of the pixels with an increase in NBP, CCAA-induced temperature change (i.e., the cooling effect of AA) is the main factor. However, CCAA-induced precipitation decrease is found to be the main factor causing NBP decrease, covering 38–57% of the NBP-decrease area (Figures 5 and 8).

At northern midlatitudes (30–60°N; Figures 8a, 8c, and 8e), simulations for the three ESMs agree with a temperature-dominated NBP increase in East Asia and the southeast United States, as well as a precipitation-dominated NBP increase in the central United States. However, large discrepancies are found among ESMs in central Eurasia. The IPSL and CSIRO simulations imply an increase of NBP mainly due to precipitation and radiation, respectively, while the GISS leads to an NBP decline due to lower precipitation from CCAA.

In contrast to the other regions, the high northern latitudes (60–90°N) showed larger area of NBP decline than increase in response to CCAA (Figure 8). This decrease is largely caused by the cooling and diming effects of aerosols, over mainly temperature- or radiation-limited ecosystems. The two factors dominate 76–81% of the high-latitude NBP-decrease region.

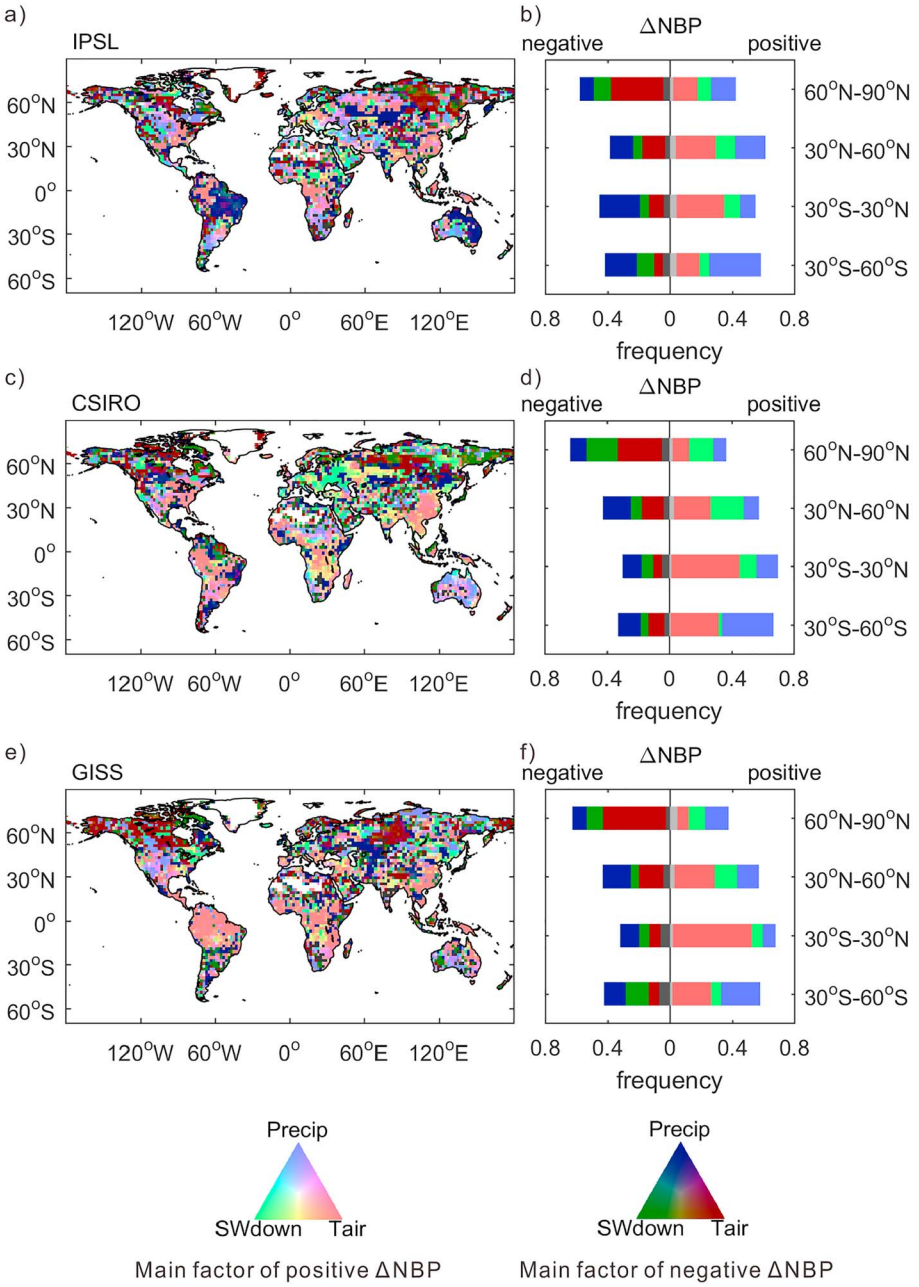

Figure 8. The spatial distribution of the main climate factors causing aerosol-induced net biome production (NBP) change. (a) The main factor for IPSL; the pixels where NBP difference is mainly contributed by *Tair*, *Precip*, and *SWdown* are presented in red, blue, and green, respectively. The bright colors indicate pixels with positive response of NBP to anthropogenic aerosols, while dark colors indicate negative response. Pixels where NBP difference cannot be explained by the three factors are shown in light gray (positive NBP response) and dark gray (negative NBP response). (b) The area statistics for the main factors (*Tair*, *Precip*, *SWdown*, and "no dominant factor" in red, blue, green, gray, respectively; positive and negative NBP responses showed in light and dark colors). (c, e) The same as (a) but for CSIRO and GISS, respectively. (d, f) The same as (b) but for CSIRO and GISS, respectively.

4. Discussion

4.1. Impacts of Aerosols on Climate

The best understood aerosol impacts on climate are through aerosol-radiation and aerosol-cloud interactions (Haywood & Boucher, 2000). Aerosol-radiation interaction occurs through the scattering and absorption of shortwave radiation. This effect often causes a negative radiative forcing because aerosols usually contribute

to enhance the Earth's albedo, except for absorbing aerosols (e.g., black carbon) in situation when the surface albedo is high (e.g., for snow or ice surfaces). The global integral of this effect results in −0.45 (−0.95 to +0.05) W/m^2 radiative forcing, although the uncertainty remains large (Boucher et al., 2013). Aerosol-cloud interactions indicate the pathways through which aerosols affect the distribution and radiative properties of clouds, mainly by acting as cloud nuclei and affecting cloud droplet size and phase (Boucher, 2015). The total radiative forcing of aerosol-cloud interactions is −0.45 (−1.2 to 0.0) W/m^2 (Boucher et al., 2013).

Both aerosol-radiation and aerosol-cloud interaction mechanisms have been incorporated in the three CMIP5 ESMs used in this study (for aerosol-cloud interaction, IPSL and GISS omitted the response of rainfall efficiency to cloud droplet size change). As a response to the aerosol-caused negative radiative forcing, cooling and diming effects are found in all of the modeled climate as expected (Figure 2). Although there is no direct observation under the *NoAA*/*NoA* scenario to validate the cooling and diming effects, such effects have been reported under high-aerosol-loading period after large volcano eruptions (Parker et al., 1996; Schwartz, 2005). However, due to different parameterizations in ESMs, the magnitudes of the cooling (0.37–0.65 °C) and diming (2.7–4.8 W/m^2) effects remain poorly constrained.

Compared with temperature and *SWdown*, precipitation has more complex responses to the radiative forcing from aerosols. At relatively short time scales, aerosols can alter precipitation by changing atmospheric radiative budget, but at longer time scales, they can meanwhile decrease precipitation by cooling the Earth's surface (Andrews et al., 2010). Here we found that all the three ESMs simulate a weak drying effect of aerosols at high latitudes (Figures 5 and S3), suggesting that the aerosol-caused surface cooling effect is predominant at this latitude. This effect is in line with Wu et al. (2013), who reported a weakened global hydrological cycle due to aerosols. At middle to low latitudes, the precipitation response to aerosols vary among ESMs, which is consistent with a recent multimodel comparison work (Samset et al., 2016). This is not surprising, because even under the same scenario (*hist*), CMIP5 ESMs already produce distinct precipitation pattern in the tropics (Ahlström et al., 2017; Mehran et al., 2014). For now, it remains difficult to say which ESM reproduced better aerosol impacts on precipitation, because no observation is available under the *NoAA*/*NoA* scenario, and any decomposition of observed climate change between several causes remains dependent on the underlying model used for the decomposition.

The climate responses discussed here are for all aerosols in GISS but only for AA for IPSL and CSIRO. The similar magnitude in the impacts from all aerosols in GISS and from AA in IPSL and CSIRO does not mean that the natural aerosols are negligible. A recent study has shown considerable feedbacks between natural aerosols and climate (Scott et al., 2018).

4.2. Response of C Fluxes

Using bias-corrected climate from CMIP5 historical experiments to force ORCHIDEE, we obtained a global C sink during 1860–2005 of 2.1–20.3 PgC, falling in the range of the IPCC AR5 estimates for the industrial period (30 ± 45 PgC; Ciais et al., 2013), which gives some confidence in the validity of this LSM to simulate historical changes in the C budget.

Compared with the positive cumulated NBP in the *hist* simulations, all the *NoAA/NoA* simulations indicate a net source during 1860–2005; that is, aerosols induce a net cumulative CO_2 sink since 1860. Similarly, Jones et al. (2003) reported that sulfate aerosols enhanced land C sink and even reversed land from C source to sink during the post-Pinatubo period. These results indicate that CCAA are an important factor for the net land C balance that may have mitigated the increase of atmospheric CO_2 concentration considerably by enhancing the terrestrial C sink. However, the magnitude of NBP increase due to CCAA remains quite uncertain (11.6–41.8 PgC during 1860–2005), which we attribute to the different aerosol treatments and climate parameterizations in the ESMs.

Despite the large range in aerosol-induced NBP increase, climate from all the ESMs leads to NBP increase mainly in the tropics and northern midlatitudes (Figure 4). This result is in line with previous studies, which showed that the interannual variation of global land C balance is mainly controlled by these regions (Cox et al., 2013; Wang et al., 2013).

A decomposition of the CCAA-caused NBP change to different fluxes revealed different mechanisms in different latitudes, when NBP is simulated with ORCHIDEE. At northern middle to high latitudes, aerosols

decreased both GPP and TER. However, the different relative strengths of the GPP and TER declines caused opposite NBP response in the two regions (Figure 4). In contrast to the consistency at middle to high latitudes, the opposite mechanism of NBP increase is found in the tropics among simulations forced by different ESM climates. This divergence can only come from the discrepancy on the aerosol-caused climate change in this region among ESMs because all C fluxes are calculated by the same LSM and the baseline difference in ESM climate has been removed (see section 2.2.2). Since the tropics contribute most to global land C flux, the mechanisms for global NBP change in response to aerosols are thus distinct among ESMs (Figure 3).

Although different ESM forcings lead to different GPP and TER responses to aerosols, all simulations agreed that the GPP change is the driver of NBP change in most regions, regardless of its sign (Figure 6). This result is in line with Koven et al. (2015), who showed a prevalent GPP-driven NBP change in ESM simulations because the substrate for respiration is ultimately originating from GPP. Nevertheless, there remain middle- to high-latitude regions where CCAA-induced NBP change is driven by TER (Figure 6). This might be due to large soil C pools in this region, which can result in strong respiration sensitivity to temperature. It should also be noted that even though most pixels in the tropics showed a GPP-driven NBP change, a small portion of TER-driven pixels can dominate the total flux at the regional scale (e.g., IPSL; Figure 4).

The net emission from land use (including instantaneous C change, long-term emissions from organic matter decomposition, and possible vegetation regrowth) is one of the most important components of land C fluxes. It determines the land C balance along with the natural C sink (C sink due to processes other than land use; Ciais et al., 2013). Our decomposition of NBP using two land use scenarios reveals that CCAA mainly affect the natural C sink, but much less land use emissions during 1966–2005. This result is robust if the period was extended to 1860–2005 (not shown). It is in line with the theoretical conclusions by Gasser and Ciais (2013). However, it is still early to draw the conclusions on how aerosols affect land use emissions because this work only includes the information on cropland extent, while land management in forests and grassland may also have considerable C consequence (Erb et al., 2018) and more impacts from CCAA.

4.3. Mechanisms of NBP Change

In this study, we found that the difference in CCAA-induced NBP change patterns at low latitudes is largely explained by aerosol-induced P-PET changes (Figure 5). For each ESM forcing, the resulting decline in NBP matches well the decrease of P-PET, indicating that C uptake is limited by water availability at middle to low latitudes. Similarly, Piao, Ciais, et al. (2009) found predominant precipitation limitation of NBP at middle to low latitudes.

How aerosols affect C fluxes not only depends on how climate is affected but may also depend on the sensitivities of C fluxes to each climate factor due to the aerosol-induced climate baseline change. Our analyses with ORCHIDEE suggest that C uptake increases in response to lower temperature and higher precipitation at low latitudes and behaves oppositely at high latitudes (Figure 7). This pattern shows high consistency among simulations using different ESM climates and between different aerosol scenarios (Figures 7 and S5–S9), indicating that aerosols do not remarkably alter the C flux sensitivities to climate during the study period. The C flux changes caused by aerosols are mainly controlled by the effect of aerosols on climate rather than on C flux sensitivities.

It should be noted that the sensitivity is based on a multilinear regression (equation (5)). Although this method has been used in previous work (Piao et al., 2013), it may fail when factors are strongly correlated, especially when there exist long-term trends in variables such as temperature, radiation (Figure 2), and CO_2. To test whether the sensitivity detected by this method is an artifact, we repeated the *hist* simulation using bias-corrected IPSL-CM5A-LR r2i1p1 climate, but keeping the atmospheric CO_2 concentration fixed at the preindustrial level. Using a similar decomposition as equation (5) but without the CO_2 term (Figure S10), we found very similar climate sensitivities as for the IPSL *hist* simulations (Figure 7), implying that the sensitivities detected by the multilinear regression is unlikely an artifact of the method.

Using the C flux sensitivities to different climate factors given by ORCHIDEE, for the first time we were able to decompose the aerosol-caused C flux change to different climate factors (Figure 8). Our results show that at middle to low latitudes, aerosol-caused cooling is responsible to most of the NBP increase, in line with previous studies showing strong sensitivity of tropical C to warming (Cox et al., 2013; Wang et al., 2013).

However, aerosols also triggered NBP decline in regions through decrease precipitation (Figure 8). The asymmetry in factors driving positive and negative NBP changes probably implies that current precipitation in some tropical regions (e.g., east Amazon) may be near or have already exceeded the threshold at which water availability begins to limit C sequestration.

Compared with those at low latitudes, the aerosol-induced NBP changes at high latitudes are more prevalently negative and can be mainly attributed to cooling and diming (Figure 8), in line with the energy limitation of C uptake in these regions (Nemani et al., 2003, Piao, Ciais, et al., 2009; Stine & Huybers, 2014). It also implies a higher temperature sensitivity of C assimilation than decomposition at high latitudes. However, C decomposition rate increases with temperature exponentially, so if temperature keeps rising, the sensitivity of TER to temperature could become stronger than that of GPP. In that case, the cooling from aerosols may cause stronger decrease in TER than in GPP and lead to positive NBP.

4.4. Advantages and Limitations of the Method

Previous studies that investigated the aerosol impacts on the C cycle also used simulations with and without aerosols (Jones et al., 2003; Mahowald et al., 2011). Using HadCM3L ESM, Jones et al. (2003) suggested a large C sink due to suppressed soil respiration in response to the cooling from CCAA. However, with CCSM3.1 ESM, Mahowald et al. (2011) gave only a small aerosol impact on global C flux. This difference implies a high sensitivity of the CCAA effect on C fluxes to the choice of one ESM forcing. In this study, we use climate data from three different ESMs, and use ensembles with three members each to further reduce the uncertainties and solidity of our results. The simulations forced by different ESMs show robust C flux response to aerosols at middle to high latitudes. However, in the tropics, there remains large divergence in CCAA-induced C flux changes among ESMs due to distinct precipitation response to aerosols. Therefore, tropical precipitation modeling is likely responsible for the different aerosol impacts found in the previous studies (Jones et al., 2003; Mahowald et al., 2011). Currently, the most efficient way to reduce the uncertainty in aerosol impacts on the C cycle should be to improve the simulation of precipitation patterns in ESMs and gain confidence on their changes in response to climate forcings (Ahlström et al., 2017).

Apart from these advantages, the current method still presents some limitations. First, the simulations in this study are all based on a single LSM, which limited the investigation of LSM-source uncertainty in aerosol impacts. Similar simulations using different LSMs are needed to test the robustness of our results. Second, besides changing climate, aerosols are able to alter the land C cycle through other pathways, such as changing light quality (Cirino et al., 2014; Gu et al., 2003; Knohl & Baldocchi, 2008; Mercado et al., 2009) and nutrient deposition (Magnani et al., 2007; Mahowald et al., 2011; Wang et al., 2017). These processes are currently absent but will be soon included in future ORCHIDEE versions to give more accurate estimations on aerosol impacts. It should also be noted that the impacts of aerosols estimated here might be somewhat different from using actual coupled simulations. This is because the LSM used here is not the ones imbedded in the CMIP5 ESMs (the ORCHIDEE LSM used here is an updated version from the one in IPSL-CM5A-LR). Also, the bias correction treatment applied and described in this study could result in different feedback terms from the CMIP5 simulations. Furthermore, the CMIP5 *hist* experiment is not fully coupled. It omitted the carbon-climate feedback due to the use of atmospheric CO_2 concentration other than CO_2 emissions as forcing.

5. Conclusions

In this study we investigated the impacts of aerosol-induced climate change on land C fluxes during the period 1860–2005 using a set of offline simulations on ORCHIDEE LSM, driven by climate under CMIP5 *hist* and *NoAA/NoA* scenarios simulated by IPSL, CSIRO, and GISS ESMs.

At the global scale, we estimated a 11.6- to 41.8-PgC NBP increase due to aerosols during the study period. Without aerosol-induced climate change, the results from the ESM used in ORCHIDEE indicate that land ecosystems would be a small cumulative source of carbon, instead of a small sink since 1860. All our simulations agree that the increased C sink occurred mainly in the tropics and north midlatitudes, while the NBP at high latitudes decreases in response to aerosols. Using a set of no land use change experiments, we show that the aerosol-induced C sink is mainly due to a change in the natural sink rather than in the land use emissions.

Using C flux sensitivities to different climate factors, we investigated the mechanisms of how aerosols affect NBP. We found that aerosol-caused cooling is responsible for most of the NBP changes. At high latitudes, GPP decrease due to aerosol cooling triggered NBP decline. At midlatitudes, cooling triggered stronger decrease in TER than in GPP, resulting in NBP increase. At low latitudes, cooling enhanced both GPP and NBP. However, this enhancement can be easily canceled when aerosols also decrease precipitation. Due to the large divergence in tropical precipitation modeling, simulations using climate from different ESMs showed uncertainty in the aerosol-caused NBP change, highlighting the need to improve precipitation modeling in ESMs.

Acknowledgments
This work was supported by the European Research Council Synergy grant ERC-2013-SyG-610028 IMBALANCE-P. We thank the ORCHIDEE group for the code and help with the ORCHIDEE model. We also thank Chris D. Jones for his constructive comments, which have helped improve this manuscript. Data used in this study can be accessed through https://esgf-node.ipsl.upmc.fr/projects/esgf-ipsl/, https://www.esrl.noaa.gov/gmd/ccgg/trends/ and https://vesg.ipsl.upmc.fr/thredds/catalog/store/p529viov/cruncep/V72_1901_2016/catalog.html.

References

Ahlström, A., Canadell, J. G., Schurgers, G., Wu, M., Berry, J. A., Guan, K., & Jackson, R. B. (2017). Hydrologic resilience and Amazon productivity. *Nature Communications*, *8*(1), 387. https://doi.org/10.1038/s41467-017-00306-z

Andrews, T., Forster, P. M., Boucher, O., Bellouin, N., & Jones, A. (2010). Precipitation, radiative forcing and global temperature change. *Geophysical Research Letters*, *37*, L14701. https://doi.org/10.1029/2010GL043991

Bellouin, N., Rae, J., Jones, A., Johnson, C., Haywood, J., & Boucher, O. (2011). Aerosol forcing in the Climate Model Intercomparison Project (CMIP5) simulations by HadGEM2-ES and the role of ammonium nitrate. *Journal of Geophysical Research*, *116*, D20206. https://doi.org/10.1029/2011JD016074

Boucher, O. (2015). *Atmospheric aerosols: Properties and climate impacts*. Netherlands: Springer.

Boucher, O., Randall, D., Artaxo, P., Bretherton, C., Feingold, G., Forster, P., et al. (2013). Clouds and aerosols. In *Climate change 2013: The physical science basis. Contribution of Working Group I to the Fifth Assessment Report of the Intergovernmental Panel on Climate Change* (pp. 571–657). Cambridge, UK and New York: Cambridge University Press.

Bowman, W. D., Cleveland, C. C., Halada, Ľ., Hreško, J., & Baron, J. S. (2008). Negative impact of nitrogen deposition on soil buffering capacity. *Nature Geoscience*, *1*(11), 767–770. https://doi.org/10.1038/ngeo339

Ciais, P., Reichstein, M., Viovy, N., Granier, A., Ogée, J., Allard, V., et al. (2005). Europe-wide reduction in primary productivity caused by the heat and drought in 2003. *Nature*, *437*(7058), 529–533. https://doi.org/10.1038/nature03972

Ciais, P., Sabine, C., Bala, G., Bopp, L., Brovkin, V., Canadell, J., et al. (2013). Carbon and other biogeochemical cycles. In *Climate change 2013: The physical science basis. Contribution of Working Group I to the Fifth Assessment Report of the Intergovernmental Panel on Climate Change* (pp. 465–570). Cambridge, UK and New York: Cambridge University Press.

Cirino, G., Souza, R., Adams, D., & Artaxo, P. (2014). The effect of atmospheric aerosol particles and clouds on net ecosystem exchange in the Amazon. *Atmospheric Chemistry and Physics*, *14*(13), 6523–6543. https://doi.org/10.5194/acp-14-6523-2014

Cox, P. M., Pearson, D., Booth, B. B., Friedlingstein, P., Huntingford, C., Jones, C. D., & Luke, C. M. (2013). Sensitivity of tropical carbon to climate change constrained by carbon dioxide variability. *Nature*, *494*(7437), 341–344. https://doi.org/10.1038/nature11882

De Rosnay, P., & Polcher, J. (1998). Modelling root water uptake in a complex land surface scheme coupled to a GCM. *Hydrology and Earth System Sciences Discussions*, *2*(2/3), 239–255. https://doi.org/10.5194/hess-2-239-1998

Ducoudré, N. I., Laval, K., & Perrier, A. (1993). SECHIBA, a new set of parameterizations of the hydrologic exchanges at the land-atmosphere interface within the LMD atmospheric general circulation model. *Journal of Climate*, *6*(2), 248–273. https://doi.org/10.1175/1520-0442(1993)006<0248:SANSOP>2.0.CO;2

Dufresne, J.-L., Foujols, M.-A., Denvil, S., Caubel, A., Marti, O., Aumont, O., et al. (2013). Climate change projections using the IPSL-CM5 Earth system model: From CMIP3 to CMIP5. *Climate Dynamics*, *40*(9–10), 2123–2165. https://doi.org/10.1007/s00382-012-1636-1

Eliseev, A. V. (2015). Impact of tropospheric sulphate aerosols on the terrestrial carbon cycle. *Global and Planetary Change*, *124*, 30–40. https://doi.org/10.1016/j.gloplacha.2014.11.005

Erb, K.-H., Kastner, T., Plutzar, C., Bais, A. L. S., Carvalhais, N., Fetzel, T., et al. (2018). Unexpectedly large impact of forest management and grazing on global vegetation biomass. *Nature*, *553*(7686), 73–76. https://doi.org/10.1038/nature25138

Flato, G., Marotzke, J., Abiodun, B., Braconnot, P., Chou, S. C., Collins, W. J., et al. (2013). Evaluation of climate models. In *Climate change 2013: The physical science basis. Contribution of Working Group I to the Fifth Assessment Report of the Intergovernmental Panel on Climate Change, Climate Change 2013*, *5* (pp. 741–866). Cambridge, UK and New York: Cambridge University Press.

Gasser, T., & Ciais, P. (2013). A theoretical framework for the net land-to-atmosphere CO_2 flux and its implications in the definition of "emissions from land-use change". *Earth System Dynamics*, *4*(1), 171–186. https://doi.org/10.5194/esd-4-171-2013

Gu, L., Baldocchi, D. D., Wofsy, S. C., Munger, J. W., Michalsky, J. J., Urbanski, S. P., & Boden, T. A. (2003). Response of a deciduous forest to the Mount Pinatubo eruption: Enhanced photosynthesis. *Science*, *299*(5615), 2035–2038. https://doi.org/10.1126/science.1078366

Haywood, J., & Boucher, O. (2000). Estimates of the direct and indirect radiative forcing due to tropospheric aerosols: A review. *Reviews of Geophysics*, *38*(4), 513–543. https://doi.org/10.1029/1999RG000078

Huete, A. R., Didan, K., Shimabukuro, Y. E., Ratana, P., Saleska, S. R., Hutyra, L. R., et al. (2006). Amazon rainforests green-up with sunlight in dry season. *Geophysical Research Letters*, *33*, L06405. https://doi.org/10.1029/2005GL025583

Hurtt, G. C., Chini, L. P., Frolking, S., Betts, R., Feddema, J., Fischer, G., et al. (2011). Harmonization of land-use scenarios for the period 1500–2100: 600 years of global gridded annual land-use transitions, wood harvest, and resulting secondary lands. *Climatic Change*, *109*(1–2), 117–161. https://doi.org/10.1007/s10584-011-0153-2

Jeffrey, S., Rotstayn, L., Collier, M., Dravitzki, S., Hamalainen, C., Moeseneder, C., et al. (2013). Australia's CMIP5 submission using the CSIRO Mk3. 6 model. *Australian Meteorological and Oceanographic Journal*, *63*(1), 1–14. https://doi.org/10.22499/2.6301.001

Jones, C. D., Cox, P. M., Essery, R. L., Roberts, D. L., & Woodage, M. J. (2003). Strong carbon cycle feedbacks in a climate model with interactive CO_2 and sulphate aerosols. *Geophysical Research Letters*, *30*(9), 1479. https://doi.org/10.1029/2003GL016867

Jung, M., Reichstein, M., Schwalm, C. R., Huntingford, C., Sitch, S., Ahlström, A., et al. (2017). Compensatory water effects link yearly global land CO_2 sink changes to temperature. *Nature*, *541*(7638), 516–520. https://doi.org/10.1038/nature20780

Knohl, A., & Baldocchi, D. D. (2008). Effects of diffuse radiation on canopy gas exchange processes in a forest ecosystem. *Journal of Geophysical Research*, *113*, G02023. https://doi.org/10.1029/2007JG000663

Koven, C. D., Chambers, J. Q., Georgiou, K., Knox, R., Negron-Juarez, R., Riley, W. J., et al. (2015). Controls on terrestrial carbon feedbacks by productivity versus turnover in the CMIP5 Earth system models. *Biogeosciences*, *12*(17), 5211–5228. https://doi.org/10.5194/bg-12-5211-2015

Krinner, G., Viovy, N., De Noblet-Ducoudré, N., Ogée, J., Polcher, J., Friedlingstein, P., et al. (2005). A dynamic global vegetation model for studies of the coupled atmosphere-biosphere system. *Global Biogeochemical Cycles*, *19*, GB1015. https://doi.org/10.1029/2003GB002199

Le Quéré, C., Andrew, R. M., Friedlingstein, P., Sitch, S., Pongratz, J., Manning, A. C., et al. (2017). Global carbon budget 2017. *Earth System Science Data Discussions*, 1–79. https://doi.org/10.5194/essd-2017-123

Luo, Y., Su, B., Currie, W. S., Dukes, J. S., Finzi, A., Hartwig, U., et al. (2004). Progressive nitrogen limitation of ecosystem responses to rising atmospheric carbon dioxide. *AIBS Bulletin*, *54*(8), 731–739.

Magnani, F., Mencuccini, M., Borghetti, M., Berbigier, P., Berninger, F., Delzon, S., et al. (2007). The human footprint in the carbon cycle of temperate and boreal forests. *Nature*, *447*(7146), 849–851. https://doi.org/10.1038/nature05847

Mahowald, N. (2011). Aerosol indirect effect on biogeochemical cycles and climate. *Science*, *334*(6057), 794–796. https://doi.org/10.1126/science.1207374

Mahowald, N., Lindsay, K., Rothenberg, D., Doney, S. C., Moore, J. K., Thornton, P., & Jones, C. (2011). Desert dust and anthropogenic aerosol interactions in the Community Climate System Model coupled-carbon-climate model. *Biogeosciences*, *8*(2), 387–414. https://doi.org/10.5194/bg-8-387-2011

Mahowald, N. M., Scanza, R., Brahney, J., Goodale, C. L., Hess, P. G., Moore, J. K., & Neff, J. (2017). Aerosol deposition impacts on land and ocean carbon cycles. *Current Climate Change Reports*, *3*(1), 16–31. https://doi.org/10.1007/s40641-017-0056-z

Mehran, A., AghaKouchak, A., & Phillips, T. J. (2014). Evaluation of CMIP5 continental precipitation simulations relative to satellite-based gauge-adjusted observations. *Journal of Geophysical Research: Atmospheres*, *119*, 1695–1707. https://doi.org/10.1002/2013JD021152

Mercado, L. M., Bellouin, N., Sitch, S., Boucher, O., Huntingford, C., Wild, M., & Cox, P. M. (2009). Impact of changes in diffuse radiation on the global land carbon sink. *Nature*, *458*(7241), 1014–1017. https://doi.org/10.1038/nature07949

Miller, R. L., Schmidt, G. A., Nazarenko, L. S., Tausnev, N., Bauer, S. E., DelGenio, A. D., et al. (2014). CMIP5 historical simulations (1850–2012) with GISS ModelE2. *Journal of Advances in Modeling Earth Systems*, *6*, 441–478. https://doi.org/10.1002/2013MS000266

Nemani, R. R., Keeling, C. D., Hashimoto, H., Jolly, W. M., Piper, S. C., Tucker, C. J., et al. (2003). Climate-driven increases in global terrestrial net primary production from 1982 to 1999. *Science*, *300*(5625), 1560–1563. https://doi.org/10.1126/science.1082750

Norby, R. J., Warren, J. M., Iversen, C. M., Medlyn, B. E., & McMurtrie, R. E. (2010). CO_2 enhancement of forest productivity constrained by limited nitrogen availability. *Proceedings of the National Academy of Sciences*, *107*(45), 19,368–19,373. https://doi.org/10.1073/pnas.1006463107

Parker, D., Wilson, H., Jones, P. D., Christy, J., & Folland, C. K. (1996). The impact of Mount Pinatubo on world-wide temperatures. *International Journal of Climatology*, *16*(5), 487–497. https://doi.org/10.1002/(SICI)1097-0088(199605)16:5<487::AID-JOC39>3.0.CO;2-J

Piao, S., Ciais, P., Friedlingstein, P., De Noblet-Ducoudré, N., Cadule, P., Viovy, N., & Wang, T. (2009). Spatiotemporal patterns of terrestrial carbon cycle during the 20th century. *Global Biogeochemical Cycles*, *23*, GB4026. https://doi.org/10.1029/2008GB003339

Piao, S., Fang, J., Ciais, P., Peylin, P., Huang, Y., Sitch, S., & Wang, T. (2009). The carbon balance of terrestrial ecosystems in China. *Nature*, *458*(7241), 1009–1013. https://doi.org/10.1038/nature07944

Piao, S., Sitch, S., Ciais, P., Friedlingstein, P., Peylin, P., Wang, X., et al. (2013). Evaluation of terrestrial carbon cycle models for their response to climate variability and to CO_2 trends. *Global Change Biology*, *19*(7), 2117–2132. https://doi.org/10.1111/gcb.12187

Piao, S. L., Friedlingstein, P., Ciais, P., Zhou, L. M., & Chen, A. P. (2006). Effect of climate and CO_2 changes on the greening of the Northern Hemisphere over the past two decades. *Geophysical Research Letters*, *33*, L23402. https://doi.org/10.1029/2006GL028205

Poulter, B., MacBean, N., Hartley, A., Khlystova, I., Arino, O., Betts, R., et al. (2015). Plant functional type classification for Earth system models: Results from the European Space Agency's Land Cover Climate Change Initiative. *Geoscientific Model Development*, *8*(7), 2315–2328. https://doi.org/10.5194/gmd-8-2315-2015

Reichstein, M., Ciais, P., Papale, D., Valentini, R., Running, S., Viovy, N., et al. (2007). Reduction of ecosystem productivity and respiration during the European summer 2003 climate anomaly: A joint flux tower, remote sensing and modelling analysis. *Global Change Biology*, *13*(3), 634–651. https://doi.org/10.1111/j.1365-2486.2006.01224.x

Rotstayn, L., Jeffrey, S., Collier, M., Dravitzki, S., Hirst, A., Syktus, J., & Wong, K. (2012). Aerosol-and greenhouse gas-induced changes in summer rainfall and circulation in the Australasian region: A study using single-forcing climate simulations. *Atmospheric Chemistry and Physics*, *12*(14), 6377–6404. https://doi.org/10.5194/acp-12-6377-2012

Samset, B., Myhre, G., Forster, P., Hodnebrog, Ø., Andrews, T., et al. (2016). Fast and slow precipitation responses to individual climate forcers: A PDRMIP multimodel study. *Geophysical Research Letters*, *43*, 2782–2791. https://doi.org/10.1002/2016GL068064

Schmidt, G. A., Kelley, M., Nazarenko, L., Ruedy, R., Russell, G. L., Aleinov, I., et al. (2014). Configuration and assessment of the GISS ModelE2 contributions to the CMIP5 archive. *Journal of Advances in Modeling Earth Systems*, *6*, 141–184. https://doi.org/10.1002/2013MS000265

Schwartz, R. D. (2005). Global dimming: Clear-sky atmospheric transmission from astronomical extinction measurements. *Journal of Geophysical Research*, *110*, D14210. https://doi.org/10.1029/2005JD005882

Scott, C., Arnold, S., Monks, S., Asmi, A., Paasonen, P., & Spracklen, D. (2018). Substantial large-scale feedbacks between natural aerosols and climate. *Nature Geoscience*, *11*(1), 44–48. https://doi.org/10.1038/s41561-017-0020-5

Sitch, S., Cox, P., Collins, W., & Huntingford, C. (2007). Indirect radiative forcing of climate change through ozone effects on the land-carbon sink. *Nature*, *448*(7155), 791–794. https://doi.org/10.1038/nature06059

Sitch, S., Huntingford, C., Gedney, N., Levy, P., Lomas, M., Piao, S., et al. (2008). Evaluation of the terrestrial carbon cycle, future plant geography and climate-carbon cycle feedbacks using five dynamic global vegetation models (DGVMs). *Global Change Biology*, *14*(9), 2015–2039. https://doi.org/10.1111/j.1365-2486.2008.01626.x

Sitch, S., Smith, B., Prentice, I. C., Arneth, A., Bondeau, A., Cramer, W., et al. (2003). Evaluation of ecosystem dynamics, plant geography and terrestrial carbon cycling in the LPJ dynamic global vegetation model. *Global Change Biology*, *9*(2), 161–185. https://doi.org/10.1046/j.1365-2486.2003.00569.x

Stine, A., & Huybers, P. (2014). Arctic tree rings as recorders of variations in light availability. *Nature Communications*, *5*(1), 3836. https://doi.org/10.1038/ncomms4836

Taylor, K. E., Stouffer, R. J., & Meehl, G. A. (2012). An overview of CMIP5 and the experiment design. *Bulletin of the American Meteorological Society*, *93*(4), 485–498. https://doi.org/10.1175/BAMS-D-11-00094.1

Thornthwaite, C. W. (1948). An approach toward a rational classification of climate. *Geographical Review*, *38*(1), 55–94. https://doi.org/10.2307/210739

Traore, A. K., Ciais, P., Vuichard, N., Poulter, B., Viovy, N., Guimberteau, M., et al. (2014). Evaluation of the ORCHIDEE ecosystem model over Africa against 25 years of satellite-based water and carbon measurements. *Journal of Geophysical Research:Biogeosciences*, *119*, 1554–1575. https://doi.org/10.1002/2014JG002638

Wang, R., Goll, D., Balkanski, Y., Hauglustaine, D., Boucher, O., Ciais, P., et al. (2017). Global forest carbon uptake due to nitrogen and phosphorus deposition from 1850 to 2100. *Global Change Biology.*, *23*(11), 4854–4872. https://doi.org/10.1111/gcb.13766

Wang, W., Ciais, P., Nemani, R. R., Canadell, J. G., Piao, S., Sitch, S., et al. (2013). Variations in atmospheric CO_2 growth rates coupled with tropical temperature. *Proceedings of the National Academy of Sciences*, *110*(32), 13,061–13,066. https://doi.org/10.1073/pnas.1219683110

Wang, X., Piao, S., Ciais, P., Friedlingstein, P., Myneni, R. B., Cox, P., et al. (2014). A two-fold increase of carbon cycle sensitivity to tropical temperature variations. *Nature*, *506*(7487), 212.

Wu, P., Christidis, N., & Stott, P. (2013). Anthropogenic impact on Earth's hydrological cycle. *Nature Climate Change*, *3*(9), 807–810. https://doi.org/10.1038/nclimate1932

Xing, J., Wang, J., Mathur, R., Wang, S., Sarwar, G., Pleim, J., et al. (2017). Impacts of aerosol direct effects on tropospheric ozone through changes in atmospheric dynamics and photolysis rates. *Atmospheric Chemistry and Physics*, *17*(16), 9869–9883. https://doi.org/10.5194/acp-17-9869-2017

Zhang, Y., Zhu, Z., Liu, Z., Zeng, Z., Ciais, P., Huang, M., et al. (2016). Seasonal and interannual changes in vegetation activity of tropical forests in Southeast Asia. *Agricultural and Forest Meteorology*, *224*, 1–10. https://doi.org/10.1016/j.agrformet.2016.04.009